SIMULATION OF PS LASER PULSES INDUCED ABSORPTION PHENOMENA IN MATERIALS

Dan Savastru[1], Roxana Savastru[2], Sorin Miclos[3] and Ion I. Lancranjan[4]
[1] National Institute of R&D for Optoelectronics – INOE 2000, dsavas@inoe.ro
[2] National Institute of R&D for Optoelectronics – INOE 2000, rsavas@inoe.ro
[3] National Institute of R&D for Optoelectronics – INOE 2000, miclos@inoe.ro
[4] National Institute of R&D for Optoelectronics – INOE 2000, ion.lancranjan@inoe.ro

ABSTRACT: The laser-induced damage in transparent or non-transparent materials represents an important active field of research as part of laser/material interactions studies. Most of research activities within this field are aiming to laser micro-processing of transparent optical materials, glasses, ceramics and metals. An example of such laser micro-processing techniques is drilling micro channels through a glass plate and drilling transverse holes through single mode optical fibre cladding and core. The latter example of research activity has an important purpose consisting of designing and manufacturing micro-nanoscale optical fibre sensors with improved capabilities. An important issue to be underlined refers to the necessity to develop simulation procedures based on accurate theoretical models of these physical processes in order to use a precise computer control of micro-processing technology.
KEY WORDS: transparent materials, laser breakdown, high intensity, damage, processing

1. INTRODUCTION

A large number of applications in the research, medical, industrial, communications and military fields strongly needs photonic and optoelectronic devices with improved characteristics and capabilities, mostly manufactured of transparent optical materials, such as semiconductors, glasses and/or ceramics. Such photonic and optoelectronic devices are manufactured using laser micro-processing [1-3]. To predict the damage threshold and to improve the design of photonic and optoelectronic components manufacturing technology are two important issues that the designer should aim to solve by an appropriate modelling and simulation [1-3]. This implies to determine the electron density distribution at the surface and in the bulk of the material [1-9]. L. V. Keldysh developed [4] analysis of damage mechanisms at short and ultrashort laser pulses timescales, which represent a basis for many simulation models [2-9]. The importance of these models comes from the fact that for laser pulse widths larger than few tens of picoseconds up to nanoseconds irreversible damage will result once sufficient energy is absorbed by the material [2-9]. In this case the absorbed laser energy is transferred to material's lattice by the excited electrons. The resulted thermal diffusion of energy causes melting and/or fracturing of the material [5-7]. The damage threshold of the material is proportional with the square root of the pulse width [7-9].

Two principal techniques are used, alone or combined, in laser micro-processing of photonic devices. The first uses shape deformation of constituent bulk material while keeping unmodified its internal structure at atomic scale [10-12]. The second bases on modifying internal structure by laser-induced breakdown at the surface and in the bulk of transparent optical materials [11-13]. The both techniques use the generation of free electrons at the surface and in the bulk of transparent materials. Laser induced damage in optical materials sets the limits in their processing [14-15]. When high intensity laser pulses are used colour centres occur, an important issue when inscribing gratings in Fibre Bragg or in Long Period Gratings [16-17]. Laser ablation micro-processing used in manufacturing in-fibre Mach-Zehnder interferometric optic sensors (to inscribe optimized gratings), largely used in smart composite materials and pathogen bacteria detection devices, benefits from these models [18-22]. This paper presents a simulation model of this kind. The model evaluates the electron generation when the material is subject to intense ultrashort laser pulses irradiation and determines thermal effects and damage thresholds. This paper presents the results obtained for Ge, at a wavelength of 635 nm, at two pulse intensities (775 GW/cm^2 and 1550 GW/cm^2) and six pulse widths (in ps range).

2. THEORY

The proposed simulation model bases on the analysis of the possible electron generation in transparent optical materials under ultrashort intensity laser pulses [2-9]. Electron generation is a part of photoionization process produced by direct excitation of electrons by the electric component of the laser field [2-9, 11-17, 23-24]. Photoionization provides

the "seed" electrons necessary for avalanche breakdown to occur for high intensity ultra-short laser pulses producing direct observable damages or for inducing sometimes useful point defects, i.e. colour centres in the optical material structure.

There are several processes involved in photon ionization, but multi photon ionization (MPI) has the highest probability to excite an electron within the material. This conclusion bases on experimentally observed damages produced in transparent optical materials and on the fact that the first harmonic photons generated by laser sources and which commonly are available for micro-processing have energy lower than the ionization potential of almost all transparent optical materials.

First we define as accurate as possible the interaction zone. It is reasonable to consider laser beam as having radial symmetry, a light radial frequency ω, peak intensity I_0, laser power P, beam radius w_0, E_p laser pulse energy and pulse repetition rate R. The peak laser intensity is defined, as a value on beam axis, by the following equation [25-26]:

$$I_0 = \frac{4E_p}{\tau \cdot w_0^2 \cdot \pi\sqrt{2\pi}} = \frac{4}{\tau \cdot w_0^2 \cdot \pi\sqrt{2\pi}} \cdot \frac{P}{R} \tag{1}$$

E_p, defined as $E_p = \frac{P}{R}$, is the laser pulse energy considered for radially symmetric beams [25-26]:

$$E_p = \int_{-\infty}^{\infty} \int_0^{2\pi} \int_0^{\infty} I(r,t) \cdot r \cdot dr \cdot d\theta \cdot dt \tag{2}$$

The laser pulse $I(r,t)$ is a Gaussian pulse, I_0 is the peak irradiance, τ is the FWHM (Full width at half maximum) pulse width, and w_0 is the beam waist: [25-26]:

$$I(r,t) = I_0 \cdot \exp\left[-2\left(\frac{r}{w_0}\right)^2\right] \cdot \exp\left[-2\left(\frac{t}{\tau}\right)^2\right] \tag{3}$$

To describing photoionization processes it is defined the electric field strength parameter F [25-26]:

$$F = \sqrt{\frac{2I}{c \cdot n \cdot \varepsilon_0}} \tag{4}$$

where I is peak laser intensity, c is the speed of light, n is refractive index, and ε_0 is the permittivity of free space.

Since the laser sources commonly used for generation of ultrashort pulses in the femtoseconds to nanoseconds range are operated at wavelengths in red and NIR spectral ranges, in the laser micro-processed transparent optical material the band gap is larger than the energy of individual incident laser photons. The laser photons incidents on a transparent optical material have more or less broad energy dispersion around a peak value [4-9]. Interaction probability for single-photon absorption in a laser-material system is highest rate to happen; if two or more lower-energy photons arrive simultaneously there is a significant probability that they will excite an electron within the material in several steps [4-9]. In the case of a transparent material with an ionization potential E_g, the necessary condition to be satisfied for MPI occurrence: simultaneous incident laser photons having slightly individual wavelengths λ_1 ... λ_n in a range $\Delta\lambda$ centred on laser source peak emission wavelength is defined as [4-9]:

$$E_g \le \hbar \cdot c \cdot \sum_{i=1}^{n} \left(\frac{1}{\lambda_i}\right) \tag{5}$$

where c is the speed of light in vacuum and $\hbar$ is the Planck constant. The photoionization rate for MPI, W_{MPI}, is defined as [4-9]:

$$W_{MPI} = \frac{2\varphi}{9\pi}\sqrt{\left(\frac{m_e \cdot \omega}{\hbar}\right)^3}\left[\sqrt{\left(2\left(\frac{E_g^*}{\hbar\omega}+1\right)-\frac{2E_g^*}{\hbar\omega}\right)}\right] \cdot \cdot e^{2\left(\frac{E_g^*}{\hbar\omega}+1\right)\left(1-\frac{e^2F^2}{4m_e\omega^2E_g}\right)\left(\frac{e^2F^2}{16m_e\omega^2E_g}\right)^{\left(\frac{E_g^*}{\hbar\omega}+1\right)}} \tag{6}$$

where E_g^* is the effective ionization potential, e is the electron charge m_e is the mass of the electron and ω is the incident laser photon angular frequency. W_{MPI} depends on the number of incident laser photons decreasing with it by a complicated law [4-9, 27-29].

3. SIMULATION RESULTS

An important goal of the simulation is to predict the total density of electrons created by high intensity laser pulses with different pulse widths. The laser induced absorption model is developed using MATLAB.

In the followings several simulation results obtained for Ge are presented (Figure 1 and Figure 2). The laser wavelength was kept the same, λ_L = 635 nm. The pulse laser peak intensity I_{peak} was considered for two values I_{peak} = 775 GW/cm^2 and I_{peak} = 1550 GW/cm^2. Another variable parameter is the laser pulse width which was considered to be in the picoseconds domain (0.21 ps, 1 ps, 2 ps, 4 ps, 6 ps and 8 ps). The other parameters considered in the developed simulation model were obtained from literature [1-3, 23-24].

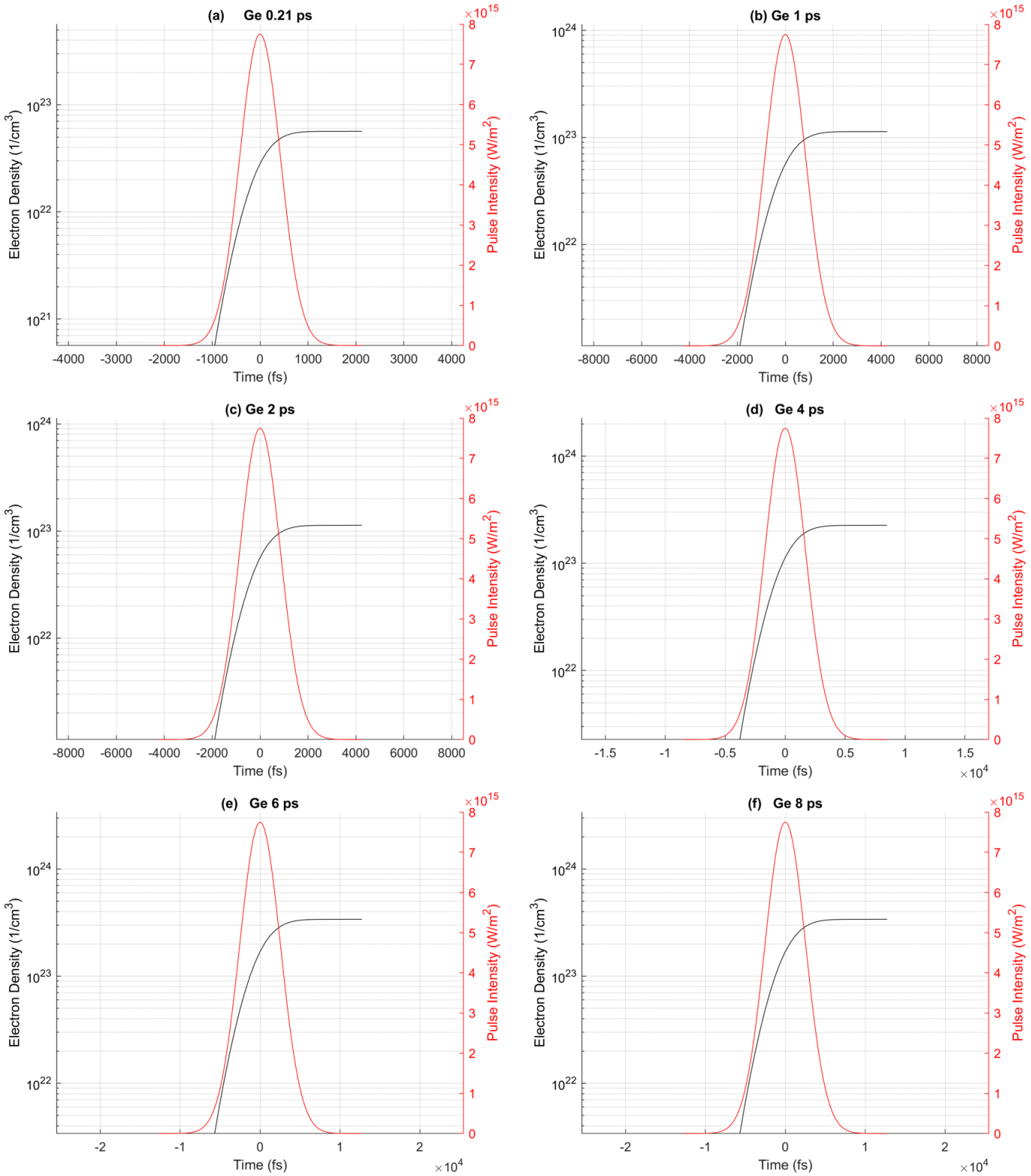

Figure 1. Total electron densities time shapes simulated at different laser pulses FWHM time duration in case of Ge. There were considered 6 values of FWHM pulse time widths, at λ = 635 nm and 775 GW/cm^2: (a) 0.21 ps; (b) 1 ps; (c) 2 ps; (d) 4 ps; (e) 6 ps; and (f) 8 ps. The laser pulse time shapes are presented in red in order to get information about time shapes of total electron densities.

In Figure 1 there are presented total densities for a peak pulse intensity of 775 GW/cm^2 and six FWHM pulse time widths. The maximum value of the total electron density (summarized in Table 1) increases almost linearly with the pulse width, as can be noticed also in Figure 3.

Table 1. Maximum values of Total Electron Densities

Pulse width [ps]	Max. Total Density [cm^{-3}]
0.21	$1.188 \cdot 10^{22}$
1	$5.657 \cdot 10^{22}$
2	$11.314 \cdot 10^{22}$
4	$22.628 \cdot 10^{22}$
6	$33.943 \cdot 10^{22}$
8	$45.258 \cdot 10^{22}$

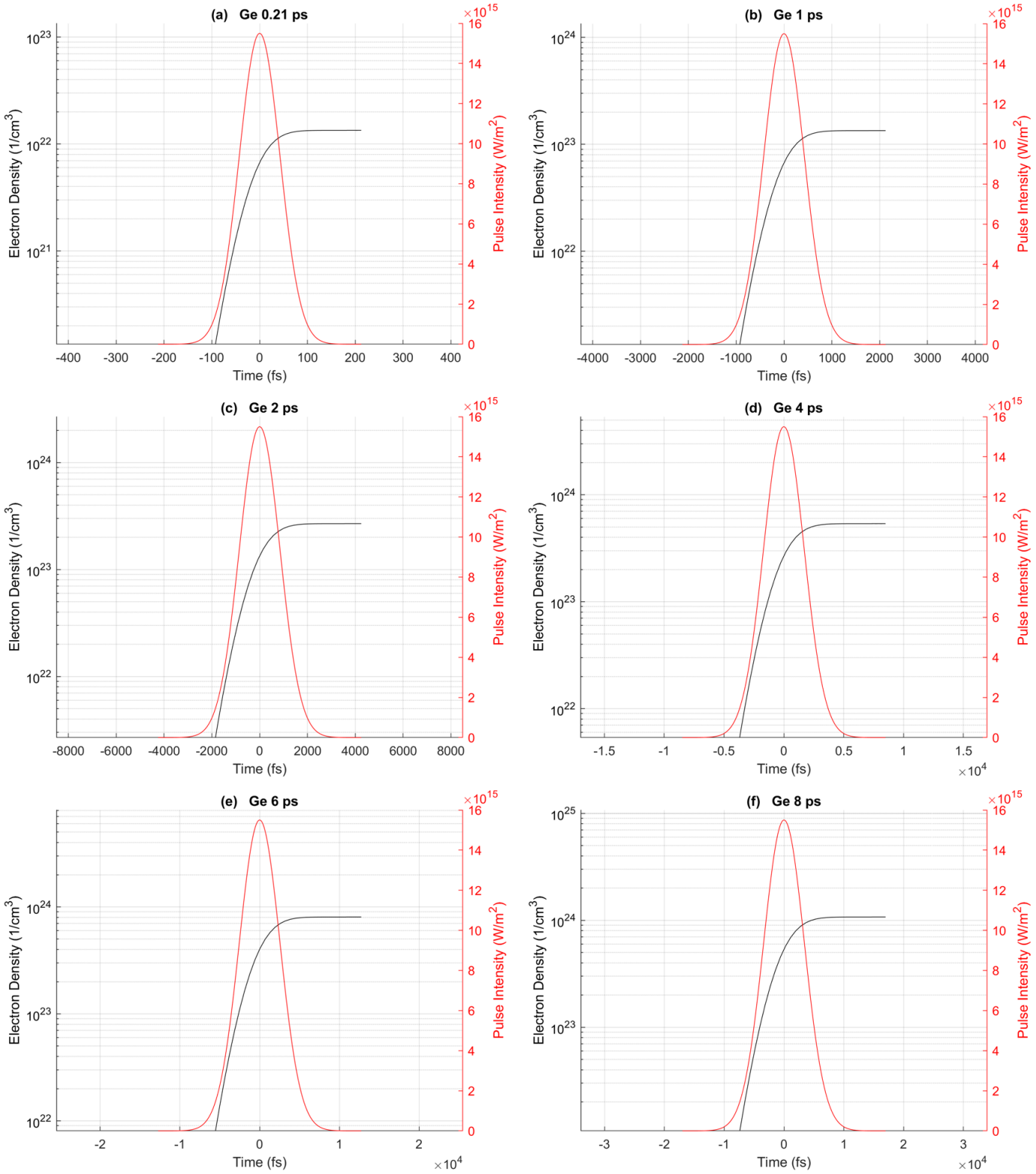

Figure 2. Total electron densities time shapes simulated at different laser pulse widths in case of Ge. There were considered 6 values of pulse widths, at λ = 635 nm and 1550 GW/cm^2: (a) 0.21 ps; (b) 1 ps; (c) 2 ps; (d) 4 ps; (e) 6 ps; and (f) 8 ps. The laser pulse time shapes are presented in red in order to get information about time shapes of total electron densities.

In Figure 2 there are presented total densities for a peak pulse intensity of 1550 GW/cm^2 and six FWHM pulse time widths. The maximum value of the total electron density (summarized in Table 2) increases almost linearly with the pulse width, as can be noticed also in Figure 3.

Table 2. Maximum values of Total Electron Densities

Pulse width [ps]	Max. Total Density [cm^{-3}]
0.21	$2.820 \cdot 10^{22}$
1	$13.429 \cdot 10^{22}$
2	$26.857 \cdot 10^{22}$
4	$53.714 \cdot 10^{22}$
6	$80.571 \cdot 10^{22}$
8	$107.428 \cdot 10^{22}$

In Fig. 1 are presented simulation results obtained in the case of Germanium for laser pulse width 0.21 ps, 1 ps, 2 ps, 4 ps, 6 ps and 8 ps, at a wavelength of 635 nm and a pulse laser peak intensity of 775 GW/cm^2. In Fig. 2 are presented simulation results obtained in the case of Germanium for laser pulse width 0.21 ps, 1 ps, 2 ps, 4 ps, 6 ps and 8 ps, at a wavelength of 635 nm and a pulse laser peak intensity of 1550 GW/cm^2. The maximal total electron density varies linearly with the laser pulse width, as it can be seen in Fig. 3, but the slope is steeper at a higher pulse laser peak intensity. Maximal values ranges from $5 \cdot 10^{22}$ cm^{-3} (for 1 ps width) to $45 \cdot 10^{22}$ cm^{-3} (for 8 ps width) in the case of a pulse laser peak intensity of 775 GW/cm^2 and from $13 \cdot 10^{22}$ cm^{-3} (for 1 ps width) to $107 \cdot 10^{22}$ cm^{-3} (for 8 ps width) in the case of a pulse laser peak intensity of 1550 GW/cm^2.

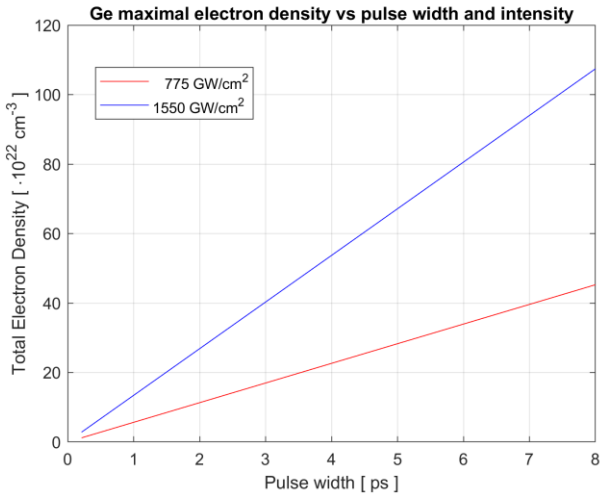

Figure 3. Ge maximal total electron density variation with laser pulse width for a peak pulse intensity of 775 GW/cm^2 (red, lower) and 1550 GW/cm^2 (blue, upper).

4. CONCLUSIONS

This study on laser induced absorption phenomena in transparent materials aims to develop a simulation tool to be used for accurate prediction of laser breakdown in such materials, the total electron density curves being included. The presented results allow the conclusion that this aim was accomplished. The presented simulation results are in fairly good agreement with the experimental ones presented in literature regarding transparent materials thermal processing and irreversible laser-induced breakdown damages [30-35]. The study is focused on the control over the induced electron density as a function of incident laser intensity geometry and time shape. The developed simulation model can be used for various transparent optical materials such as different optical ceramics, crystals, chalcogenide, germanate, tellurite and silicate glasses.

5. ACKNOWLEDGEMENTS

This research is supported by the Core Program, under the support of ANCS, project no. PN 19-18.01.02 and by the MANUNET grant no. MNET17/NMCS0042.

6. REFERENCES

1. Xu, S.Z., Zu, X.T., Yuan, X.D., Localized CO2 laser treatment and post-heating process to reduce the growth coefficient of fused silica surface damage, *Chin. Opt. Lett.*, Vol. 9, No. 6, pp. 061405, (2011).
2. Miclos, S., Savastru, D., Lancranjan, I., Numerical Simulation of a Fiber Laser Bending Sensitivity, *Rom. Rep. Phys.*, Vol. 62, No. 3, pp. 519-527, (2010).
3. Savastru, D., Savastru, R., Miclos, S., Lancranjan I., Numerical analysis of photonic crystal waveguide, *J. Ovonic Res.*, Vol. 9, No. 5, pp. 147-155, (2013).
4. Keldysh, L.V., Ionization in the field of a strong electromagnetic wave, *Sov. Phys. Jetp-USSR*, Vol. 20, No. 5, pp.1307-1314, (1965).
5. Smith, H., Jensen, H.H., *Transport phenomena*, Clarendon Press eds., Oxford, (1989).
6. Wong, J., Ferriera, J.L., Lindsey, E.F., Haupt, D.L., Hutcheon, I.D., Kinney, J.H., Morphology and microstructure in fused silica induced by high fluence ultraviolet (355 nm) laser pulses, *J. Non-Cryst. Solids*, Vol. 352, No. 3, pp. 255–272, (2006).
7. Qi, H.J., Zhu, M.P., Fang, M., Shao, S.Y., Wei, C.Y., Yi, K., Shao, J.D., Development of high-power laser coatings, *High Power Laser Sci. Eng.*, Vol. 1, No. 1, pp. 36–43, (2013).
8. Vignes, J.R.M, Soules, T.F., Stolken, J.S., Settgast, R.R., Elhadj, S., Matthews, M.J., Thermomechanical Modeling of Laser-Induced Structural Relaxation and Deformation of Glass: Volume Changes in Fused Silica at High Temperatures, *J. Am. Ceram. Soc.*, Vol. 96, No. 1, pp. 137–145, (2013).
9. Reif, J., Costache, F., Henyk, M., Pandelov, S.V., Ripples revisted: non-classical morphology at the bottom of femtosecond laser ablation craters in transparent dielectrics, *Appl. Surf. Sci.*, Vol. 197-198, pp. 891–895, (2002).
10. Savastru, D., Miclos, S., Savastru, R., Lancranjan, I., Analysis of optical microfiber thermal processes. *Rom. Rep. Phys.*, Vol. 67, No. 4, pp. 1586–1596, (2015).
11. Tsibidis, G.D., Barberoglou, M., Loukakos, P.A., Stratakis, E., Fotakis, C., Dynamics of ripple formation on silicon surfaces by ultrashort laser

pulses in subablation conditions, *Phys. Rev. B*, Vol. 86, No. 11, pp. 115316, (2012).
12. Bonse, J., Rosenfeld, A., Krüger, J., On the role of surface plasmon polaritons in the formation of laser-induced periodic surface structures upon irradiation of silicon by femtosecond-laser pulses, *J. Appl. Phys.*, Vol. 106, pp. 104910, (2009).
13. Rohloff, M., Das, S.K., Höhm, S., Grunwald, R., Rosenfeld, A., Krüger, J., Bonse, J., Formation of laser-induced periodic surface structures on fused silica upon multiple cross-polarized double-femtosecond-laser-pulse irradiation sequences, *J. Appl. Phys.*, Vol. 110, pp. 014910, (2011).
14. Das, S.K., Messaoudi, H., Debroy, A., McGlynn, E., Grunwald, R., Multiphoton excitation of surface plasmon–polaritons and scaling of nanoripple formation in large bandgap materials, *Opt. Mater. Express*, Vol. 3, No. 10, pp. 1705–1715, (2013).
15. Birnbaum, M., Semiconductor surface damage produced by ruby lasers, *J. Appl. Phys.*, Vol. 36, pp. 3688–3689, (1965).
16. Keilmann, F., Bai, Y.H., Periodic surface structures frozen into CO2 laser-melted quartz, *Appl. Phys. A*, Vol. 29, No. 1, pp. 9–18, (1982).
17. Temple, P. A., Soileau, M.J., Polarization charge model for laser-induced ripple patterns in dielectric materials, *IEEE J. Quantum Elect.*, Vol. 17, No. 10, pp. 2067–2072, (1981).
18. Miclos, S., Savastru, D., Savastru, R., Lancranjan, I.I., Numerical analysis of Long Period Grating Fibre Sensor operational characteristics as embedded in polymer, *Composite Structures*, Vol. 183, No. SI, pp. 521–526, (2018).
19. Savastru, D., Miclos, S., Savastru, R., Lancranjan, I.I., Study of thermo-mechanical characteristics of polymer composite materials with embedded optical fibre, Composite Structures, Vol. 183, No. SI, pp. 682–687, (2018).
20. Gouveia, C.A.J., Baptista, J.M., Jorge, P.A.S., Refractometric Optical Fiber Platforms for Label Free Sensing, Chapter 13 in *Current Developments in Optical Fiber Technology*, pp. 345-373, INTECH eds., (2014).
21. Gautier, S.M., Blum, L.J., Coulet, P.R., Fibre-optic biosensor based on luminescence and immobilized enzymes: Microdetermination of sorbitol, ethanol and oxaloacetate, *J. Biolumin. Chemilumin.*, Vol. 5, No. 1, pp. 57-63, (1990).
22. Tian, Y., Wang, W., Wu, N., Zou, X., Wang, X., Tapered Optical Fiber Sensor for Label-Free Detection of Biomolecules, *Sensors*, Vol. 11, No. 4), pp. 3780-3790, (2011).
23. Crisp, M.D., Boling, N.L., Dube, G., Importance of Fresnel reflections in laser surface damage of transparent dielectrics, *Appl. Phys. Lett.*, Vol. 21, No. 8, pp. 364–366, (1972).
24. Zeng, X., Mao, X.L., Greif, R., Russo, R.E., Experimental investigation of ablation efficiency and plasma expansion during femtosecond and nanosecond laser ablation of silicon, *Appl. Phys. A*, Vol. 80, No. 2, pp. 237–241, (2005).
25. Hodgson, N., Weber, H., *Laser Resonators and Beam Propagation. Fundamentals, Advanced Concepts and Applications*, 2nd edition, Springer Science and Business Media Inc. eds., New York, (2005).
26. Siegman, A.E., *Lasers*, University Science Books eds., Sausalito, California, (1986).
27. Obara, G., Shimizu, H., Enami, T., Mazur, E., Terakawa, M., Obara, M., Growth of high spatial frequency periodic ripple structures on SiC crystal surfaces irradiated with successive femtosecond laser pulses, *Opt. Express*, Vol. 21, No. 22, pp. 26323–26334, (2013).
28. Deng, Z., Eberly, J.H., Multiphoton absorption above ionization threshold by atoms in strong laser fields, *JOSA B*, Vol. 2, No. 3, pp. 486-493, (1985).
29. Letokhov, V.S., *Laser photoionization spectroscopy*, Academic Press eds., (1987).
30. Dyer, P. E., Farley, R. J., Giedl, R., Karnakis, D. M., Excimer laser ablation of polymers and glasses for grating fabrication, *Appl. Surf. Sci*., Vol. 96–98, pp. 537–549, (1996).
31. Yu, Z. K., He, H. B., Qi, H. J., Fang, Z., Li, D. W., Characteristics of 355 nm laser damage in bulk materials, *Chinese Phys. Lett.*, Vol. 30, No. 6, Art. No. 067801, (2013).
32. Stuart, B. C., Feit, M. D., Rubenchik, A. M., Shore, B. W., Perry, M. D., Laser-Induced Damage in Dielectrics with Nanosecond to Subpicosecond Pulses, *Phys. Rev. Lett*., Vol. 74, pp. 2248-2251, (1995).
33. Liu, X., Du, D., Mourou, G., Laser ablation and micromachining with ultrashort laser pulses, *IEEE J. Quantum Elect.*, Vol. 33, No. 10, pp. 1706-1716, (1997).
34. Gattass, R. R., Cerami, L. R., Mazur, E., Micromachining of bulk glass with bursts of femtosecond laser pulses at variable repetition rates, *Opt. Express*, Vol. 14, No. 12, pp. 351-354, (2006).
35. Osellame, R., Taccheo, S., Marangoni, M., Ramponi, R., Laporta, P., Polli, D., De Silvestri, S., Cerullo, G., Femtosecond writing of active optical waveguides with astigmatically shaped beams, *JOSA B*, Vol. 20, No. 7, pp. 1559-67, (2003).